THE IMPACT OF TERRAIN CORRECTION OF POLARIMETRIC SAR DATA ON GLACIER CHANGE DETECTION

Vahid Akbari[1]*, Yngvar Larsen*[2]*, Anthony P. Doulgeris*[1]*, and Torbjørn Eltoft*[1,2]

[1]Department of Physics and Technology, University of Tromsø, 9037,Tromsø, Norway
[2]Northern Research Institute (Norut), Tromsø, Norway

ABSTRACT

This paper investigates the impact of terrain correction on change detection results. We firstly assess the effects of topography on radar brightness and show how we can produce the radiometrically terrain corrected multilook complex (MLC) covariance data. Next, changes on radar cross section as a function of polarization states due to azimuth slope variations will be studied. Finally experimental results on glacier dataset are shown by focusing on change detection results before and after terrain corrections.

Index Terms— Synthetic aperture radar, radiometric terrain correction, azimuth slope correction, glacier change detection, polarization.

1. INTRODUCTION

Spaceborne synthetic aperture radar (SAR) instruments, operating independently of weather and light, have proven to be a very useful tool for multi-temporal image analysis. However, surface topography has influence on the geometric and radiometric quality of SAR images [1]. In addition, terrain azimuth slope variations lead to changes in radar cross sections as a function of polarization states [2]. Hence, before analyzing the data, terrain correction is a prerequisite for intercomparisions of multi-temporal SAR images. The developed method for terrain correction of polarimetric SAR (PolSAR) data in this paper utilizes the pixel area normalization on each element of the covariance matrix. Moreover, azimuth slope correction is immediately following after radiometric correction. Accurate backscatter estimates enable more robust use of the retrieved values for some applications such as land cover classification, monitoring of changes, edge detection and retrieval of geophysical parameters.

2. DATA AND STUDY AREA

Two SAR images from the ASAR sensor onboard the Envisat satellite are used in this paper. These scenes have been acquired over the Kongsvegen glacier, Svalbard from May 2004 and April 2006, with different acquisition configurations. These images consists of data in alternating polarization (AP) mode from descending orbit and in VV/VH and HH/HV polarizations with look angles IS5 and IS3. A DEM of 20 m grid-spacing covering all of Svalbard was also available.

3. POLARIMETRIC SAR DATA

A full-polarimetric imaging radar measures the amplitude and phase of backscattering signals in the four combinations of the linear receive and transmit polarizations: hh, hv, vh, and vv. These signals form a 2×2 complex scattering matrix, associated with each resolution cell in the image, which relates the incident and the scattered electric fields [3]. Assuming that the reciprocity principle is satisfied, the backscattering of a monostatic PolSAR system is characterized by the complex scattering vector

$$\vec{\mathbf{k}} = [S_{hh}, \sqrt{2}S_{hv}, S_{vv}]^T, \tag{1}$$

where the elements represent the three complex backscattering coefficients of each polarization channels and the superscript T denotes the matrix transpose. The vector $\vec{\mathbf{k}}$ is the single-look complex (SLC) representation of polarimetric SAR data. Usually, polarimetric data are transformed into the form of multilooked sample covariance matrices in order to reduce speckle noise, i.e.,

$$\mathbf{C} = \frac{1}{L}\sum_{l=1}^{L} \vec{\mathbf{k}}_l \vec{\mathbf{k}}_l^H \tag{2}$$

where L is the nominal number of looks used for averaging, the superscript H means complex conjugate transpose. Hence, after multilooking, each pixel in the image is a realization of the $d \times d$ stochastic matrix variable denoted $\mathbf{C}$, where d is the dimension of the scattering vector, and the image is referred to as the MLC image.

4. RADAR BACKSCATTER

The radar backsatter (β) of a given target measured in slant range plane for linear polarizations (p, q) can be obtained

Thanks to the research council of Norway for funding.

from the elements of scattering vector as follows:

$$\beta_{pq} = 4\pi |S_{pq}|^2. \quad (3)$$

Both β_{pq} and S_{pq} are functions of wave frequency, viewing geometry, wave polarization, object geometrical structure, and object dielectric properties [3]. The area normalized scattering vector in the slant range plane is obtained from:

$$\vec{\mathbf{k}}_{\beta^0} = \frac{\vec{\mathbf{k}}_{\beta}}{A_{\beta}}, \quad (4)$$

where A_β represents the scattering area which contributes to the recorded signal.

5. TERRAIN CORRECTION

Terrain topography influences both the position of each given point on the Earth's surface and the brightness of the radar return in radar geometry [4, 5]. In this study, we analyze a method to generate terrain corrected PolSAR images for time series analysis. The procedure is implemented in three steps:

- Geometric terrain correction (GTC)
- Radiometric terrain correction (RTC)
- Azimuthal slope correction (ASC)

5.1. Geometric Terrain Correction (GTC)

The objective of the SAR geocoding is to reconstruct the imaging geometry to find the corresponding position on the Earth for each image pixel. Since the satellite state vector is known from orbit information, the position of each SAR pixel is estimated on a given earth model by solving the range-Doppler equations [6]. Due to geometrical distortions caused by the side looking geometry, a one-to-one relation does not exist between radar and map geometries [1]. Therefore, a DEM is used to perform an accurate geocoding and then geometric terrain correction of terrain induced distortions.

5.2. Radiometric Terrain Correction (RTC)

The normalization of PolSAR imagery for systematic terrain variations is required for meaningful single sensor multi-track intercomparisions and time series analysis [1]. Although the position of the backscatter estimate has been corrected by the GTC, the radiometry of the geocoded image remains on the slant range plane. Therefore, *radiometric terrain correction* (RTC) is applied to correct distortions due to the side-looking geometry of SAR systems and hill-slope modulations [7]. In this study, we first normalize the scattering coefficients with respect to the β_0 reference area (A_β) according to Eq. (4) and then reduce the influence of the terrain topography on covariance matrices. To perform a precise radiometric correction, we need to estimate the changing scattering area in the map geometry, caused by the terrain topography, parameterized by the projection angle Ψ [7]. Provided that data are already calibrated, all elements of covariance matrix in Eq. (2) can be radiometrically corrected to the ground range area by

$$\mathbf{C}_{RTC} = \frac{\cos(\Psi)}{L} \sum_{l=1}^{L} (\vec{\mathbf{k}}_{\beta^0})_l (\vec{\mathbf{k}}_{\beta^0})_l^H = \cos(\Psi) \cdot \mathbf{C}_{\beta^0}, \quad (5)$$

where the Ψ is the angle between the surface normal and the image plane normal [7] and the projection factor can be estimated as follows:

$$\cos(\Psi) = \sin(\theta_L)\cos(u) + \cos(\theta_L)\sin(u)\sin(v), \quad (6)$$

where u and v are the terrain slope and aspect with respect to the sensor azimuth direction and θ_L is the local incidence angle at the scattering surface. All matrix values now correspond to the σ^0 backscatter coefficient. The conventional radiometric normalization method, which relies on the local incidence angle only, is adequate for flatlands or for pixels with zero slope ($u = 0$) in the Eq. (6). The expected results give us "flattened" SAR radiometry. Since different scattering mechanisms have different sensitivity to terrain topography, RTC is not sufficient for the polarimetric applications (eg., target decompositions) to produce reliable results for scattering characteristics [2].

5.3. Azimuthal Slope Correction (ASC)

Another problem which makes changes in radar cross sections is caused by azimuth slopes. It was shown by *Lee et al.* [2] that this effect is a function of the polarization state. The goal of the second-order radiometric terrain correction, the *azimuthal slope correction* (ASC), is to correct PolSAR data from distortions induced by terrain azimuth slope variations. In the case of rugged terrain areas, the orientation angle (OA), which is the angle of rotation about the line of sight, is shifted from zero. These shifts make the covariance matrix *reflection asymmetrical* and can be compensated based on the derived OA in [2]. The derivation is accurate for airborne radar systems. We need to adjust it using local incidence angles estimated in the geocoding step in order to apply it to spaceborne PolSAR data as follows:

$$\tan(\nu) = \frac{\tan(\omega)}{-\tan(\gamma)\cos(\theta_L) + \sin(\theta_L)} \quad (7)$$

where ω is the azimuth slope angle, γ is the slope angle in the ground range direction. Target decomposition-based methods are other alternatives to estimate the OA [2]. For dual-pol data with 2×2 covariance matrix data, the OA has to be derived from the DEM because the information contained in the dual-pol data is not adequate to estimate OA by target-decomposion methods. The radiometrically corrected MLC

data can be compensated by OA of ν as follows:

$$\mathbf{C}_{ASC} = R(\nu)\mathbf{C}_{RTC}R^T(\nu), \tag{8}$$

where the rotation matrix $R(\nu)$ for dual-pol data is given by

$$R(\nu) = \begin{bmatrix} \cos(\nu) & \sin(\nu) \\ -\sin(\nu) & \cos(\nu) \end{bmatrix}. \tag{9}$$

The PolSAR data are now ready for quantitative image analysis, such as target decompositions, surface cover classification or change detection.

6. $\mathcal{U}$-MRF FOR CLUSTERING OF POLSAR DATA

An unsupervised, non-Gaussian, contextual segmentation method is used that combines an advanced statistical distribution with spatial contextual information for MLC data. It is based on a Markov random field (MRF) model that integrates a $\mathcal{U}_d$-distribution for the PolSAR data statistics conditioned to each image cluster and a Potts model for the spatial context [8]. Specifically, the proposed algorithm is constructed based upon the expectation maximization (EM) algorithm. The resulting algorithm works in an iterative manner to jointly address parameter estimation of the $\mathcal{U}_d$-distribution and the spatial context model, and also minimization of the energy function [9].

7. EXPERIMENTAL RESULTS

The SLC data are geocoded and multilooked to produce MLC images with 30 m resolution and 24-looks. The reconstruction of radar geometry is done not only to derive the geocoding look-up tables, but also to derive various geometrical parameters for each ground point such as local incidence angle, the projection angle and to generate the layover-shadows mask. The pixels affected by the geometrical distortions are mainly located at slopes larger than 40 degrees. Kongsvegen glacier has a gentle surface slope of 0.5-5 degrees, which reduces slope-induced effects in the SAR images except at high slope regions where the brightness caused by topography may cause misinterpreted class boundaries. The projection factor is shown in Fig. 1(c). The backscatter coefficient is reduced when using the projection factor to radiometrically correct the covariance matrix. The negative projection factors (the projection angles larger than 90 degree), correspond to the dark blue areas in Fig. 1(c) and red areas in the slope map. These areas mostly are affected by layover and in the geocoding step have to be masked out, as seen in the Fig. 1(b).

We use the DEM-derived OAs to compensate the terrain azimuth slope variation in this study. By estimating the OA for the data (Fig. 1(d)), we observe that for the rugged-terrain areas surrounding the glacier, the polarization shifts are more significant. For most natural backscatter media, azimuthal symmetry holds meaning that cross correlation between co- and cross-polarized channels are uncorrelated. However, Azimuth slope variations may induce correlation between channels. Of course, the incoherent imaging system of the ASAR sensor in AP mode may also compound this issue resulting in reflection asymetrical MLC data. Subsequently, the OA compensation over images leads to reflection symmetric covariance matrix data.

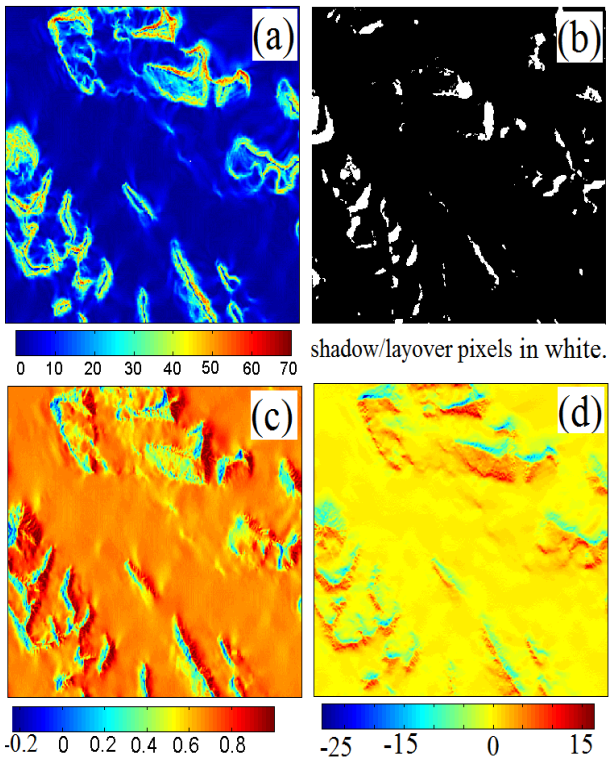

Fig. 1. Terrain correction parameters of the covered area in the map geometry. (a) slope angle map (b) shadow/layover mask produced from the geocoding step (c) projection factor (d) polarization orientation angle.

To demonstrate the effect of both RTC and ASC, the profile along center line of the glacier was plotted for the two images with different geometries. The original backscatter coefficient, RTC and ASC values are shown with red, green and blue lines respectively. The total backscatter power (Span=$C_{11} + C_{22}$) in Fig. 2 does not change significantly after OA compensation except some small changes for the pixels located at the higher azimuth slopes. A mask is applied to isolate the glacier pixels for segmentation. Unsupervised contextual non-Gaussian segmentation was then performed using the $\mathcal{U}$-MRF classifier over uncorrected and terrain corrected PolSAR dataset. The segmented images are compared, and changes in the location of boundaries between glacier facies are thus detected and marked. This is done without and with terrain corrections to see how much significant changes happen in the results. The results are shown in the Fig. 3. As seen in Fig. 3(a), the the boundary between the superimposed

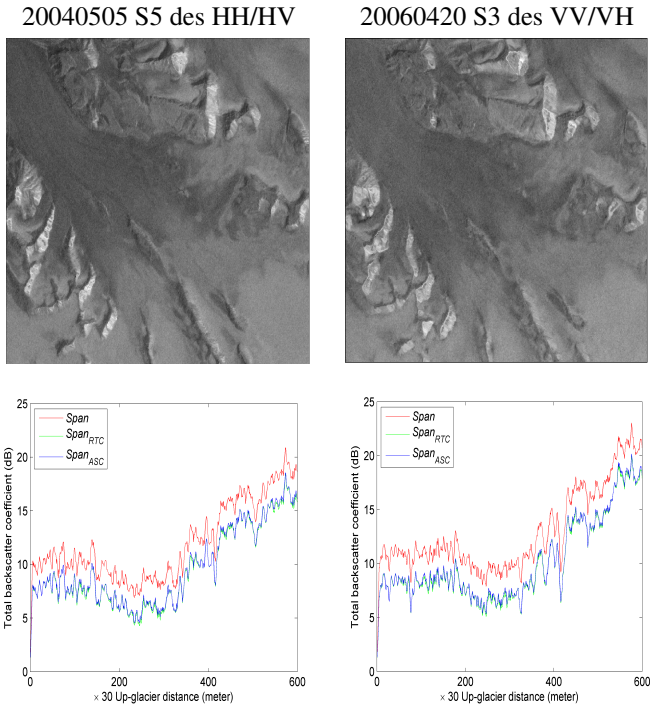

Fig. 2. Span images after terrain corrections. The effect of terrain correction on PolSAR data before radiometric normalization, after radiometric normalization and after polarization compensation with DEM along center line of the glacier.

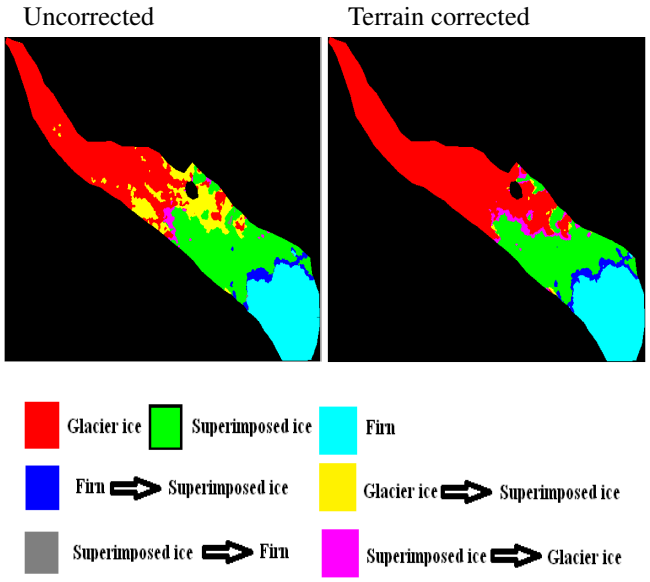

Fig. 3. Change detection results before (left) and after (right) terrain corrections. The colors show the change detection classes between two images.

ice and glacier ice is influenced by topography and the uncorrected changes are not realistic. But after terrain correction, the change detection results are found to be more reasonable.

8. CONCLUSIONS

In this paper, we studied the impacts of radiometric terrain correction of polarimetric SAR data on change detection results. We first performed the radiometric normalization in map geometry and then compensate the polarimetric SAR data for terrain azimuth slope variation. We applied an unsupervised clustering method to segment the images. Finally, we did post-classification change detection analysis based on the segmented images on a pixel-by-pixel based analysis. Based upon these change maps performed with and without terrain corrections, we compared results to investigate the impacts of terrain corrections on results.

9. REFERENCES

[1] D. Small, "Flattening Gamma: Radiometric Terrain Correction for SAR Imagery," *IEEE Trans. Geosci. Remote Sens.*, vol. 49, no. 8, pp 3081-3093, Aug. 2011.

[2] J. S. Lee and T. L. Ainsworth, "The Effect of Orientation Angle Compensation on Coherency Matrix and Polarimetric Target Decompositions," *IEEE Trans. Geosci. Remote Sens.*, vol. 49, no.1, pp. 53-64, Jan. 2011.

[3] J.-S. Lee and E. Pottier, "Polarimetric Radar Imaging: From Basics to Applications," ser. *Optical Science and Engineering*, Boca Raton, USA: CRC Press, 2009, no. 143.

[4] T. Bayer, R.Winter, and G. Schreier, "Terrain Influences in SAR Backscatter and Attempts to Their Correction," *IEEE Trans. Geosci. Remote Sens.*, vol. 29, no. 3, pp. 451-462, May 1991.

[5] A. Loew and W. Mauser, "Generation of Geometrically and Radiometrically Terrain Corrected SAR Image Products," *Remote Sens. of Env.*, vol. 106, pp. 337-349, 2007.

[6] J. C. Curlander, and R. N. McDonough, "Synthetic Aperture Radar Systems and Signal Processing," *John Wiley and Sons, Inc*, New York, 1991.

[7] L. M. H. Ulander, "Radiometric Slope Correction of Synthetic-Aperture Radar Images," *IEEE Trans. Geosci. Remote Sensing*, vol. 47, no. 7, pp. 1115-1122, Sep, 1996.

[8] A. Doulgeris, V. Akbari, and T. Eltoft, "Automatic PolSAR Segmentation with the $\mathcal{U}$-Distribution and Markov Random Fields," Proc. *EUSAR 2012*, pp. 183-186, 23-26 April, 2012

[9] G. Celeux, F. Forbes, and N. Peyrand, "EM Procedures Using Mean Field-Like Approximations for Markov Model-Based Image Segmentation," *Pattern Recognition*, vol. 36, no. 1, pp. 131-144, 2003.